VISER
www.viserdata.com

RESEARCH AND APPLICATION OF MATERIALS SCIENCE

ISSN 2661-4464(online) 2661-4456(print)
Volume 7 No. 2 2025

COMPANY INTRODUCTION

Viser Technology Pte. Ltd. was founded in Singapore with branch offices in both Hebei and Chongqing, China. Viser focuses on publishing scientific and technological journals and books that promote the exchange of scientific and technological findings among the research community and around the globe. Despite being a young company, Viser is actively connecting with well-known universities, research institutes, and indexation database, and has already established a stable collaborative relationship with them. We also have a group of experienced editors and publishing experts who are dedicated to publishing high-quality journal and book contents. We offer the scholars various academic journals covering a variety of subjects and we are committed to reducing the hassles of scholarly publishing. To achieve this goal, we provide scholars with an all-in-one platform that offers solutions to every publishing process that a scholar needs to go through in order to show their latest finding to the world.

Research and Application of Materials Science

Publisher: Viser Technology Pte. Ltd.

ISSN: 2661-4464(online)
2661-4456(print)

Frequency: Semi-annual

Add.: 195 Pearl's Hill Terrace, #02-41,
Singapore 168976

https://www.viserdata.com/

Research and Application of Materials Science

Volume 7 No.2 (2025)

CONTENTS

Viser Technology Pte. Ltd.
Research and Application of Materials Science
DOI: 10.33142/rams.v7i2.19667

Research Article Open Access

Carbonized Polymer Dots-Induced Multivalent Hydrogen-Bonding Networks in Hydrogel Electrolytes for High-Performance Low-Temperature Zinc-Ion Batteries

Yuming LIU[†], Xin JI[†], Siyu ZHANG, Yangyu SUN, Haizhu SUN[*]

Key Laboratory of Sustained and Advanced Functional Materials, College of Chemistry, Northeast Normal University, Changchun Jilin 130024, P. R. China

[*]***Corresponding Author:*** *Haizhu SUN, E-mail: sunhz335@nenu.edu.cn*
[†]***Co-first Authors:*** *Yuming LIU and Xin JI*

Abstract

Aqueous zinc-ion batteries (AZIBs) are considered promising candidates for next-generation energy storage systems owing to their intrinsic safety, low cost, high theoretical capacity (820 mAh g^{-1}), and environmental friendliness. However, the excessive free water in conventional aqueous electrolytes severely compromises low-temperature performance due to the inherently high freezing point of water. Moreover, water-induced parasitic reactions on the Zn metal anode, including hydrogen evolution, corrosion, and passivation, inevitably lead to poor electrode reversibility and limited cycling stability, thereby hindering their practical applications in low-temperature environments. Herein, carbonized polymer dots (CPDs) with abundant surface functional groups are introduced to regulate the hydrogen-bonding environment within the hydrogel electrolyte. The CPDs effectively disrupt the original hydrogen-bonding network of free water and reconstruct multivalent hydrogen-bonding interactions among CPDs, free water, and polyacrylamide (PAM) chains. Such a strategy immobilizes free water and converts it into bound water, thereby significantly depressing the freezing point of the electrolyte. In addition, CPDs facilitate rapid Zn^{2+} transport under low-temperature conditions while simultaneously suppressing Zn dendrite growth and undesirable side reactions. Furthermore, the influence of CPDs content on the electrochemical performance was systematically investigated by tuning the volume ratio between CPDs and PAM. When the CPDs volume ratio reached 0.3, the Zn||Zn symmetric cell exhibited highly stable cycling performance for 800 h (2 mA $cm^{-2,}$ 1 mAh cm^{-2}) at -25°C. This work provides a feasible strategy for the rational design of high-performance low-temperature resistance hydrogel electrolytes for advanced zinc-ion batteries.

Keywords: *Carbonized polymer dots (CPDs); polyacrylamide (PAM); low-temperature resistance*

1 Introduction

Currently, aqueous zinc-ion batteries (AZIBs) have attracted extensive attention owing to their high safety, environmental benignity, and high energy density [1-4]. However, several critical challenges, including uncontrolled zinc dendrite growth, hydrogen evolution reactions, corrosion, and internal short circuits, still severely hinder their practical applications and cycling stability [5-8]. Although gel electrolytes can effectively suppress electrolyte leakage and reduce the risk of internal short circuits, issues associated with sluggish ion transport and insufficient inhibition of zinc dendrites remain unresolved [9,10].

To address these limitations, various strategies have been proposed, including the construction of composite electrodes, the introduction of electrolyte additives, and the development of composite gel electrolytes [11]. Among these approaches, composite gel electrolytes have attracted considerable interest because of their high thermal stability, excellent electrode/electrolyte interfacial contact, and enhanced ionic conductivity derived from improved ion transport kinetics [12,13]. For example, Zhuang et al. developed an acidic PAMPS/PAM hydrogel electrolyte in which abundant sulfonic acid groups acted as proton reservoirs to maintain a stable acidic environment and facilitate cation transport [14]. In another study, Wan and co-workers fabricated TPU/PVA composite gel electrolytes through solution blending and phase inversion methods, where the formation of a semi-interpenetrating polymer network synergistically enhanced mechanical stability and ion transport capability. Furthermore, hydrogen-bonding interactions between abundant polar groups and hydrogen ions effectively reduced free proton activity, thereby suppressing zinc dendrite growth and

Received: October 30, 2025; Accepted: December 18, 2025

electrode corrosion while maintaining high ionic conductivity [15]. Nevertheless, current studies on AZIBs capable of simultaneously achieving high energy density and long-term cycling stability under low-temperature conditions remain limited, highlighting the urgent need for efficient Low-Temperature gel electrolytes [16].

Polyacrylamide (PAM) has been widely employed as a gel electrolyte matrix because of its low cost, facile fabrication process, and favorable ionic transport properties. Its three-dimensional polymer network promotes the homogeneous distribution of Zn^{2+} while maintaining good ionic conductivity. However, the intrinsic antifreezing capability of PAM remains inadequate, and its relatively weak mechanical strength cannot effectively suppress zinc dendrite growth during prolonged cycling [17,18]. In this context, carbonized polymer dots (CPDs), as an emerging class of zero-dimensional carbon-based nanomaterials, offer new opportunities for the design of advanced low-temperature gel electrolytes. CPDs possess a carbonaceous core enriched with abundant tunable surface-active sites and excellent dispersibility. More importantly, the abundant oxygen-containing functional groups on CPDs can reconstruct hydrogen-bonding interactions within the electrolyte and regulate Zn^{2+} deposition behavior, thereby enabling more uniform zinc plating/stripping processes and improved electrochemical stability under low-temperature conditions [19].

Herein, a composite hydrogel electrolyte based on polyacrylamide (PAM) and carbonized polymer dots (CPDs) was constructed, as illustrated in Figure 1. The CPDs, derived from glucose and ethanol, are enriched with abundant hydroxyl and carboxyl functional groups, which can effectively disrupt the original hydrogen-bonding network of free water. Through the synergistic interactions among CPDs, PAM chains, and water molecules, a multivalent hydrogen-bonding network is reconstructed within the electrolyte, thereby immobilizing free water and converting it into bound water to reduce the freezing point of the electrolyte [20,21]. Meanwhile, the reconstructed hydrogen-bonding environment effectively regulates the Zn^{2+} solvation structure and facilitates rapid Zn^{2+} transport under low-temperature conditions, resulting in more uniform Zn deposition behavior and suppressed zinc dendrite growth as well as parasitic side reactions [22]. Furthermore, the influence of CPDs content on the electrochemical performance was systematically investigated to determine the optimal composition. Benefiting from the optimized hydrogen-bonding network and enhanced ion transport behavior, the assembled Zn||Zn symmetric cell with the optimized gel electrolyte achieved stable cycling performance for 800 h at -25 ℃ under a current density of 2 mA cm^{-2} and an areal capacity of 1 mAh cm^{-2}. This work provides an effective strategy for the rational design of high-performance low-temperature hydrogel electrolytes for advanced aqueous zinc-ion batteries.

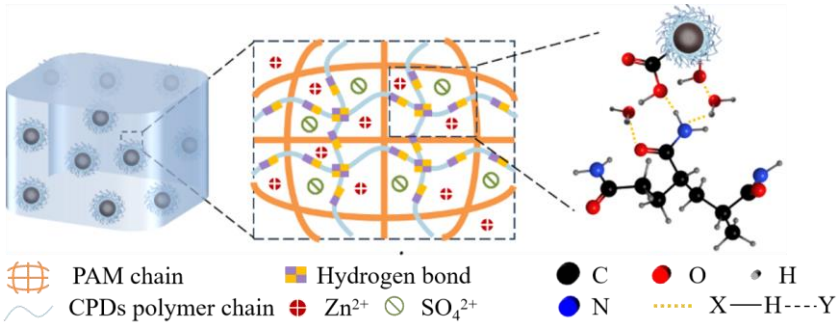

Figure 1 Specific schematic diagram of the PAM-CPDs

2 Experiment Section

2.1 Preparation of CPDs

0.75 g of glucose was weighed and dissolved in 60 mL of ethanol. The mixture was stirred at room temperature for ten minutes, and then the resulting solution was transferred to a sealed high-pressure reactor lined with polytetrafluoroethylene (PTFE). The solvothermal reaction was conducted under high pressure at 180 ℃ for 12 h. After cooling to room temperature, the solution containing CPDs was obtained.

2.2 Preparation of hydrogel

The synthesis was carried out with volume ratios of aqueous solution to carbon dot solution of 10:0, 9:1, 7:3, 5:5, and 3:7. For each ratio, 5.7512 g of $ZnSO_4 \cdot 7H_2O$was added to the corresponding volume of purified water (10 mL, 9 mL, 7 mL, 5 mL, and 3 mL, respectively), and the mixtures were stirred at room temperature.

Subsequently, the carbon dot solution was added in the specified proportions, along with 2 g of AM (acrylamide monomer) and 2.5 mg of MBAA (N, N'-methylenebisacrylamide, the crosslinker). After the mixture was stirred for 30 minutes at room temperature, APS (ammonium persulfate, the initiator) was added, and stirring was continued until all solids were dissolved. The stirred solution was then poured into the gap of a glass plate secured with clamps and was reacted at 60 ℃ for 2 h to obtain the desired gel. The gel thickness was

determined by the glass plate gap; a thickness of 1 mm was obtained, with a measurement error not exceeding 0.01 mm. The synthesized gel was subsequently pressed into uniformly sized discs with a diameter of 15.8 mm using a presser.

2.2.1 Assembly of cells

The coin-shaped CR2032 Zn||Zn symmetric battery is fabricated from two zinc foils and a gel electrolyte containing different PAM-CPDs formulations.

2.2.2 Types of instruments and tests

The characteristic functional groups in CPDs electrolytes with varying concentrations were characterized using an Agilent Technologies Cray 630 FTIR (Fourier Transform Infrared) spectrometer; Raman spectroscopy was employed to characterize the surface functional groups in CPDs electrolytes with different concentrations. Electrochemical impedance spectroscopy (EIS) measurements were performed using the CHI660E electrochemical workstation, with an amplitude of 5 mV and a frequency range from 10^{-2} Hz to 10^{6} Hz. The hydrogen evolution reaction (HER) was investigated by linear scanning voltammetry (LSV) at a scanning rate of 1 mV s^{-1}, within the scanning ranges of 0 to -0.5 V and 0 to 3 V.

3 Results and discussion

3.1 Structure characterization of CPDs

First, the gel electrolyte additive CPDs were characterized. As shown in Fig. 2a, the CPDs solution exhibits a uniformly dispersed deep brown color. Under 365 nm ultraviolet irradiation (Fig. 2b), the CPDs solution displays bright blue fluorescence, demonstrating the excellent fluorescent properties of the synthesized CPDs. To investigate the structure and morphology of CPDs, XRD analysis was first conducted. As shown in Fig. 2c, a broad diffraction peak centered at approximately 25 ° is observed, which can be attributed to amorphous carbon, indicating that the CPDs consist of carbonized polymer dots with carbon nuclei as the core structure. To further identify the surface functional groups of the CPDs, FT-IR and XPS analyses were subsequently performed. As shown in Fig. 2d, characteristic absorption peaks corresponding to O-H, C=O, C=C, and C-O-C functional groups are clearly observed, confirming the successful introduction of abundant oxygen-containing functional groups onto the CPDs surface. Furthermore, XPS measurements were carried out to further verify the surface chemical composition and bonding states of the CPDs. The high-resolution C 1s spectrum shown in Fig. 2f can be deconvoluted into four characteristic peaks corresponding to C-C/C-H (284 eV), C-O-C (286 eV), O=C-O (289 eV), and -OH (291 eV), respectively. Meanwhile, the high-resolution O 1s spectrum in Fig. 2g reveals characteristic peaks attributed to C-O (532 eV), O=C-O (533 eV), and -OH (535 eV), which is consistent with the FT-IR results. The above results demonstrate that CPDs with a carbon core and surfaces rich in oxygen-containing functional groups, such as -OH and -COOH, were successfully synthesized. These abundant surface functional groups can effectively disrupt the hydrogen-bonding interactions of free water and further establish multiple hydrogen-bonding interactions with both water molecules in the hydrogel electrolyte and PAM polymer chains. Consequently, the proportion of bound water is increased, thereby enhancing the low-temperature adaptability of the hydrogel electrolyte.

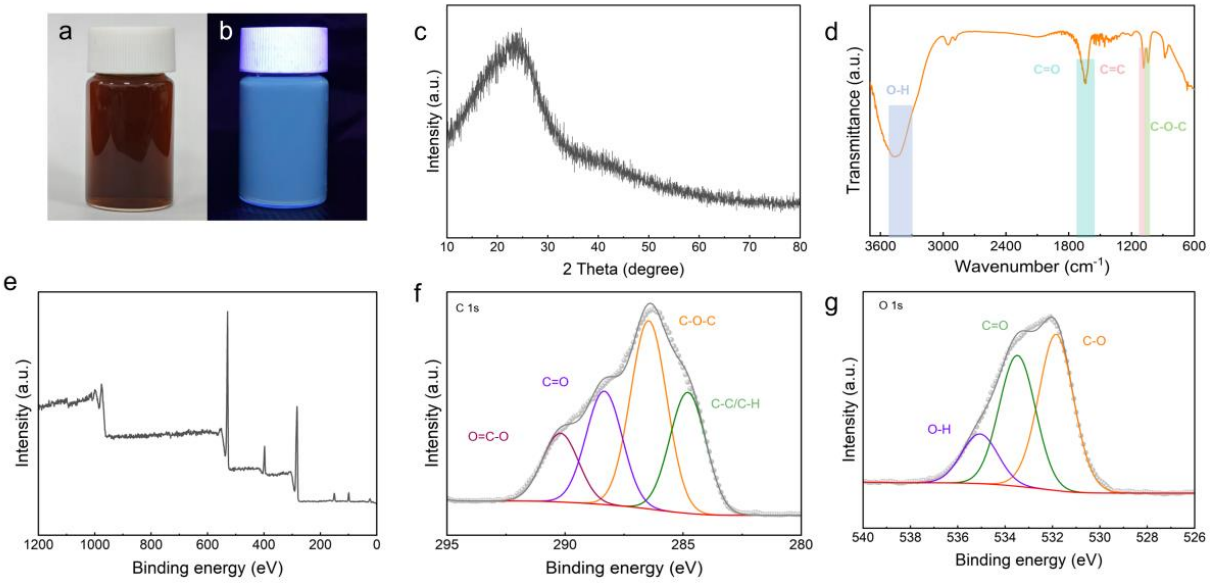

Figure 2 (a-b) Photographs of the CPDs solution under visible light and 365 nm UV irradiation, respectively. (c) XRD pattern of CPDs. (d) FT-IR spectrum of CPDs. (e) XPS survey spectrum of CPDs. High-resolution XPS spectra of (f) C 1s and (g) O 1s for CPDs.

3.2 Morphology of PAM-CPDs gel electrolytes

As shown in Fig. 3a, the AM precursor solution was initially colorless and transparent before polymerization at room temperature. With the gradual increase in the volume ratio of the CPDs solution, the color of the precursor solution progressively deepened and became increasingly brown. Subsequently, the precursor solution was polymerized at 60 ℃ for 2 h. After polymerization, the obtained electrolyte remained stable regardless of bottle inclination, confirming the successful formation of the gel electrolyte. After storage at -25 ℃ for 2 h, the pure PAM electrolyte transformed into a white opaque solid. This phenomenon was mainly attributed to the precipitation of $ZnSO_4$ crystals at low temperatures, which severely hindered ion transport within the electrolyte. In contrast, freezing was no longer observed in the PAM-0.3CPDs, PAM-0.5CPDs, and PAM-0.7CPDs gel electrolytes with increasing CPDs content, indicating that the incorporation of CPDs effectively enhanced the structural stability and low-temperature adaptability of the gel electrolyte. As shown in Fig. 3b, the synthesized gel electrolytes were cut into circular discs with a diameter of approximately 15.8 mm (error ≤ 0.1 mm) and an initial thickness of 1 mm. The detailed thickness measurements are presented in Fig. 3c. Considering that the thickness of the external protective film was 0.066 mm, the actual thicknesses of the gel electrolytes were calculated to be 0.855, 0.851, 0.854, 0.852, and 0.753 mm, respectively. However, when the CPDs content reached 70%, the gel electrolyte exhibited obvious deformation and could no longer be pressed into a regular circular sheet. This result indicates that excessive CPDs significantly increased the viscosity of the PAM hydrogel electrolyte, thereby hindering Zn^{2+} transport within the electrolyte network.

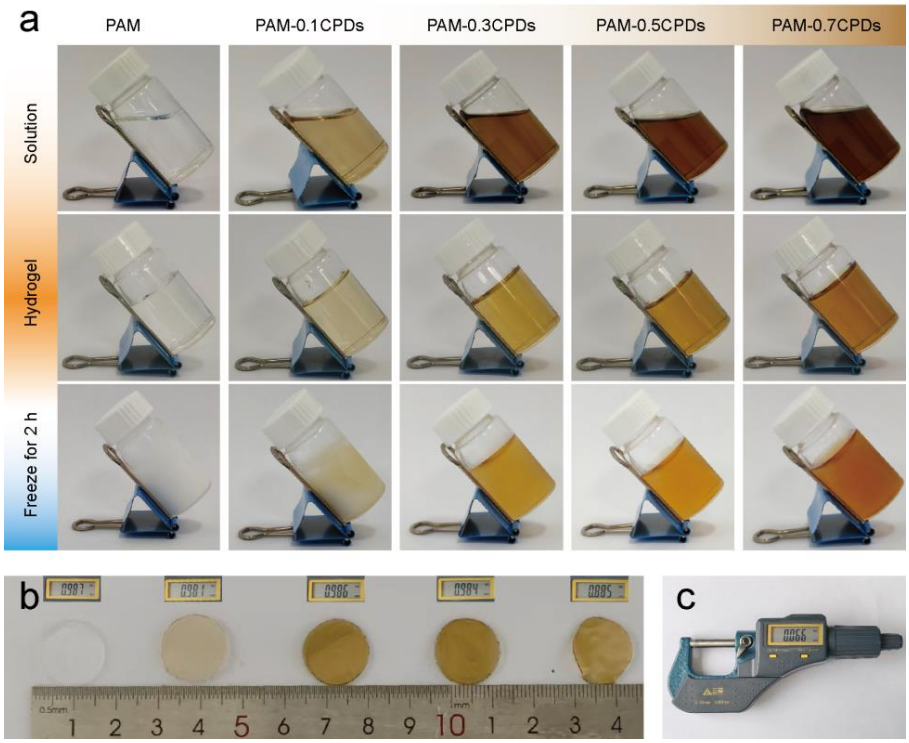

Figure 3 (a) Photos of the synthesized material under room temperature, heated, and frozen conditions; (b) Photos of the diameter of the gel electrolyte; (c) Thickness of the film outside the gel electrolyte (single layer). Supplementary thickness diagrams for each gel electrolyte are embedded in (b).

3.3 Structure PAM-CPDs gel electrolytes

As shown in Fig. 4a, the freezing points of pure PAM, PAM-0.1CPDs, PAM-0.3CPDs, and PAM-0.5CPDs are -9.5 ℃, -14.84 ℃, -20.33 ℃, and -26.85 ℃, respectively. These results demonstrate that the freezing point of the PAM–CPDs composite gel electrolyte gradually decreases with increasing CPDs content. Compared with pure PAM, the composite gel electrolytes exhibit significantly enhanced low-temperature adaptability, which is consistent with the observations shown in Fig. 3a. As shown in the FT-IR spectra in Fig. 4b, the absorption peaks in the range of 3300-3200 cm^{-1} correspond to the stretching vibrations of O-H groups. With increasing CPDs content, the hydroxyl absorption peak gradually shifts toward lower wavenumbers, while the characteristic absorption peak located at 1700-1650 cm^{-1}, corresponding to the bending vibrations of water molecules, gradually shifts toward higher wavenumbers. These results indicate that the hydroxyl and carboxyl groups on CPDs effectively disrupt the hydrogen-bonding interactions of free water, thereby

promoting the formation of multiple hydrogen bonds among free water, PAM chains, and CPDs. As shown in Fig. 4c, the Raman spectra reveal that the intensities of the characteristic C-OH peak (1360-1450 cm^{-1}) and C-O peak (1150-1050 cm^{-1}) gradually increase with increasing CPDs content, confirming the successful introduction of abundant oxygen-containing functional groups by CPDs. Meanwhile, the C-C skeletal vibration peak (1000-950 cm^{-1}) exhibits gradual enhancement accompanied by a blue shift, while the -CH_2 bending vibration peak (900-800 cm^{-1}) also shows enhanced intensity and a blue shift. In addition, the C-C-O skeletal vibration peak (650-550 cm^{-1}) displays enhanced intensity together with a red shift. These results further demonstrate that multiple hydrogen-bonding interactions are formed among CPDs, PAM chains, and free water molecules. Consistent with the FT-IR results, these interactions provide the structural basis for the formation of a cross-linked network, thereby enhancing the overall performance and low-temperature stability of the gel electrolyte.

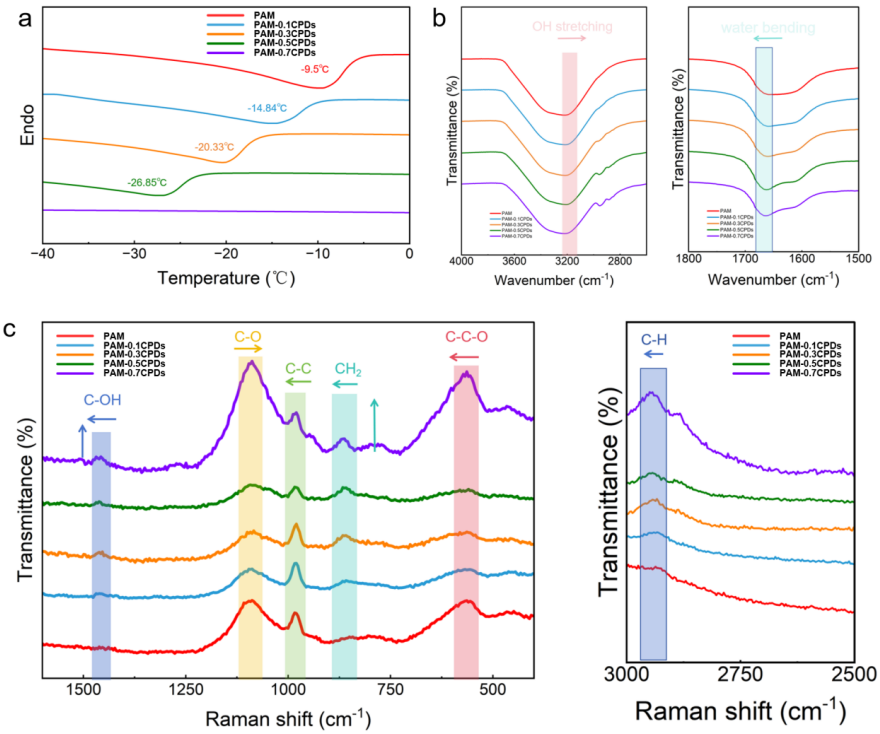

Figure 4 (a) DSC curves of the PAM, PAM-0.1CPDs, PAM-0.3CPDs, PAM-0.5CPDs, and PAM-0.7CPDs gel electrolytes; (b) Infrared spectroscopy spectra; (c) Raman spectroscopy spectra.

3.4 Electrochemical performance testing

To evaluate the electrochemical performance of the gel electrolytes and determine the optimal CPDs content, rate capability and long-term cycling tests were conducted using Zn||Zn symmetric cells. As shown in Fig. 5a, the rate performance was investigated at a fixed areal capacity of 1 mAh cm^{-2} while varying the current density from 0.1 to 10 mA cm^{-2}, followed by returning to 1 mA cm^{-2} for continuous cycling. The pure PAM electrolyte exhibited obvious voltage polarization, and the overpotential increased significantly during the middle and later stages of cycling. The total cycling durations of PAM, PAM-0.1CPDs, PAM-0.3CPDs, PAM-0.5CPDs, and PAM-0.7CPDs were 109 h, 75 h, 140 h, 143 h and 55 h, respectively. These results indicate that the introduction of CPDs effectively improves the electrochemical stability of the PAM electrolyte under varying current densities and reduces the risk of short-circuit failure. In particular, the PAM-0.3CPDs electrolyte exhibited the lowest overpotential, suggesting optimized Zn^{2+} transport kinetics and more stable Zn plating/stripping behavior. Long-term cycling tests were further performed at a fixed current density of 2 mA cm^{-2} and an areal capacity of 1 mAh cm^{-2}. As shown in Fig. 5b, at -5 ℃, the pure PAM electrolyte maintained stable cycling for only 200 h, whereas the cycling lifetimes of PAM-0.1CPDs, PAM-0.3CPDs, and PAM-0.5CPDs reached 346, 742, and 349 h, respectively. In contrast, PAM-0.7CPDs failed to sustain stable long-term cycling under the same conditions. Among all samples, PAM-0.3CPDs exhibited the longest cycling lifespan and the most stable electrochemical performance. Furthermore, as shown in Fig. 5d, when the temperature was decreased to -25 ℃, the pure PAM electrolyte solidified completely and lost its ionic conductivity. Under these conditions, the cycling lifetimes of PAM-0.1CPDs, PAM-0.3CPDs, and PAM-0.5CPDs were

6 h, 800 h and 186 h, respectively, whereas neither PAM nor PAM-0.7CPDs could maintain stable cycling. These results further confirm that the optimized hydrogen-bonding network induced by CPDs effectively enhances the low-temperature adaptability and interfacial stability of the hydrogel electrolyte.

3.5 Investigation of electrolyte properties

First, linear sweep voltammetry (LSV) was employed to evaluate the electrochemical stability window of the gel electrolytes during the charging/discharging process. As shown in Fig. 6a, the PAM and PAM-0.7CPDs electrolytes exhibited inflection points at 2.44 V, whereas the inflection points of PAM-0.1CPDs, PAM-0.3CPDs, and PAM-0.5CPDs were located at 2.46, 2.56, and 2.48 V, respectively. These results indicate that the incorporation of CPDs can effectively suppress oxygen evolution reactions and broaden the electrochemical stability window of the electrolyte. Among all samples, PAM-0.3CPDs exhibited the highest decomposition voltage, demonstrating the most effective suppression of parasitic reactions. Subsequently, electrochemical impedance spectroscopy (EIS) measurements were conducted to investigate the ion transport behavior of the gel electrolytes with different CPDs contents. As shown in Fig. 6b, the charge-transfer resistance of the composite electrolytes was significantly lower than that of the pure PAM electrolyte, indicating that the incorporation of CPDs effectively facilitates Zn^{2+} transport kinetics and promotes rapid interfacial electrochemical reactions. Furthermore, the ionic conductivity of the gel electrolytes was evaluated based on the EIS results. As shown in Fig. 6c, the charge-transfer resistance initially decreased and then increased with increasing CPDs content. Correspondingly, the ionic conductivities of PAM, PAM-0.1CPDs, PAM-0.3CPDs, PAM-0.5CPDs, and PAM-0.7CPDs were calculated to be 10.4, 13.1, 38.6, 10.9, and 8.3 mS cm^{-1}, respectively, as summarized in Fig. 6d. Notably, PAM-0.3CPDs exhibited the highest ionic conductivity, further confirming that the optimized incorporation of CPDs significantly enhances ion transport kinetics within the hydrogel electrolyte.

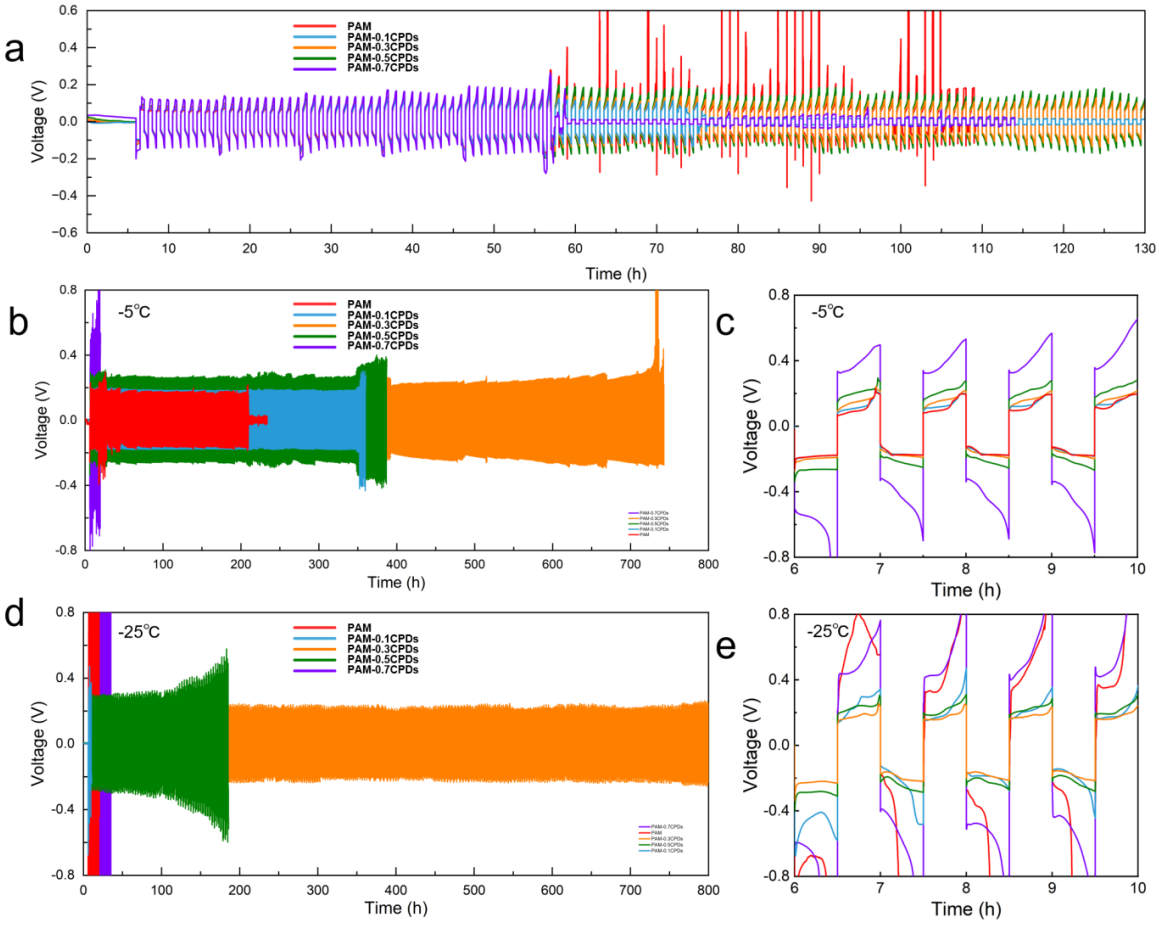

Figure 5 (a) Rate performance test curves of Zn||Zn symmetric batteries using gel electrolytes composed of various PAM formulations: PAM, PAM-0.1CPDs, PAM-0.3CPDs, PAM-0.5CPDs, and PAM-0.7CPDs; (b) Long-cycle performance test curves of the battery at-5℃; (c) Amplified view of the long-cycle performance test from 6 to 10 hours shown in (b); (d) Long-cycle performance test curves of the battery at-25℃; (e) Amplified view of the long-cycle performance test from 6 to 10 hours shown in (d).

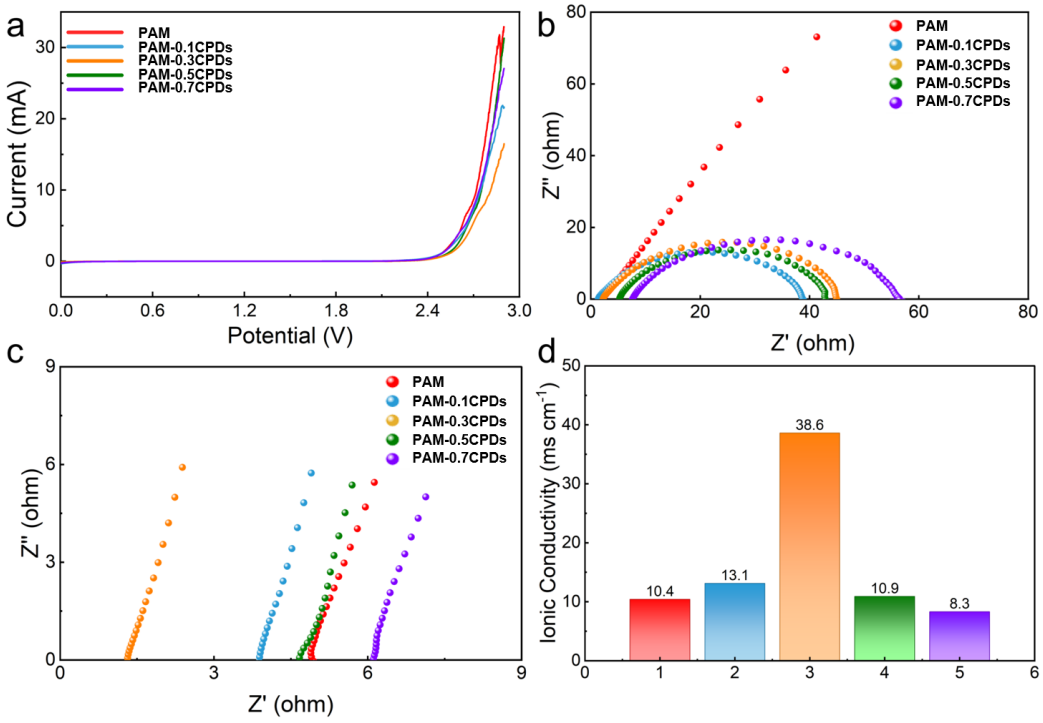

Figure 6 (a) linear sweep voltammetry (LSV) test, (b) Electrochemical impedance spectroscopy (EIS) test curves, (c) Ion conductivity test curves of Zn||Zn symmetric cells using the PAM, PAM-0.1CPDs, PAM-0.3CPDs, PAM-0.5CPDs, and PAM-0.7CPDs gel electrolytes; (d) Bar chart showing the ion conductivity values of each gel electrolyte.

4 Conclusion

In summary, a low-temperature composite hydrogel electrolyte based on polyacrylamide (PAM) and carbonized polymer dots (CPDs) was successfully constructed for high-performance aqueous zinc-ion batteries. Benefiting from the abundant hydroxyl and carboxyl functional groups on the CPDs surface, a multivalent hydrogen-bonding network was effectively established among CPDs, PAM chains, and water molecules, which significantly disrupted the hydrogen-bonding interactions of free water and promoted the conversion of free water into bound water. As a result, the freezing point of the hydrogel electrolyte was markedly reduced, while Zn^{2+} transport kinetics and interfacial stability were simultaneously improved under low-temperature conditions. Moreover, the incorporation of CPDs effectively regulated the Zn^{2+} solvation structure, suppressed hydrogen evolution side reactions and zinc dendrite growth, and enhanced the ionic conductivity of the electrolyte. Among all samples, PAM-0.3CPDs exhibited the optimal electrochemical performance, delivering stable cycling for 800 h at -25 ℃ under a current density of 2 mA cm^{-2} and an areal capacity of 1 mAh cm^{-2}. This work provides an effective strategy for the rational design of advanced low-temperature hydrogel electrolytes for high-performance aqueous zinc-ion batteries.

Acknowledgements: This work was supported by Jilin Province Science and Technology Development Plan Project (International cooperation 20240402073GH), the National Natural Science Foundation of China(22275030).

References

[1] Chen Jinhui, Tao Yingqing, Zhang Tianyu, et al.Toward durable wide-temperature Zn-MnO_2 batteries: A polarized dual-crosslinked hydrogel electrolyte for concurrent anode and cathode stabilization [J]. Chemical Engineering Journal, 2026(535):175539.

[2] Kang Jiahong, Wu Bozhi, Chen Shuning, et al. Solvent-induced biphasic phase separated hydrogels: Synergistic energy dissipation for softness, ultra-tough and shape recovery [J]. Chemical Engineering Journal, 2026(529):172732.

[3] Wu Yuying, Xie Dan, Liu Chang, Synergistic effect of hydrogen bond network and molecular cage enables wide-temperature quasi-solid zinc-ion batteries [J]. Chemical Engineering Journal, 2026(529):173033.

[4] Xiong Peixun, Kang Yingbo, Yao nan, et al. Zn-Ion Transporting, In Situ Formed Robust Solid Electrolyte Interphase for Stable Zinc Metal Anodes over a Wide Temperature Range [J]. ACS Energy Letters, 2023, 8 (3):1613–1625.

[5] Zhang Pengfei, Li Xinjie, Li Ziyue, et al. A highly stable zinc–air battery based on a non-alkaline agar gel electrolyte [J].

Energy & Environmental Science, 2026, 19 (3), 1069–1079.
[6] Gao Rui, Wang Jifeng, Song Yuanyuan, Polymer-Salt Effects with Enhanced Eutectic Behavior in Hydrogel Electrolytes for Aqueous Zinc Batteries at −70 ℃ [J]. Advanced Functional Materials, 2026,36 (2):e14585.
[7] Zhu Baonian, Yan Yuefeng, Hong Jingzhe, et al. Accelerated proton transport modulates dynamic hydrogen bonding networks in eutectic gel electrolytes for low-temperature aqueous Zn-metal batteries [J]. Journal of Energy Chemistry, 2025(109):325–336.
[8] Yang Ruiqiang, Zhang Yangqian, Liao Yaqi, et al. Double-network hybrid hydrogel electrolyte suppresses zinc dendrites and vanadium dissolution for durable zinc-metal batteries [J]. Energy Storage Materials, 2026(88):105097.
[9] Wu Runhai, Wang Ran, Yang Shaopei, et al. Bio-inspired hyaluronic acid enhanced dual-network hydrogel electrolyte unlocks dendrite-free Zn deposition and exceptional cycling stability in flexible zinc ion batteries [J]. Chemical Engineering Journal, 2026(530):173528.
[10] Liu Ziming, Zhang Xuke, Zhang Heng, et al. Construction of Homogeneously Porous Composite Hydrogel Electrolyte for Dendrite-Free Aqueous Zinc-Ion Batteries: An Alkali-Etched Graphitized-Carbon Nitride Induced Polymerization Strategy [J]. Advanced Functional Materials, 2026(0):e75312.
[11] Gou Lei, Zhu Lin, Wang Wei, et al. From Physical Cross-Linking to Tailored Phosphorylation: Unlocking High-Performance and Biocompatible Xanthan-Konjac Hydrogels for Zinc-Ion Batteries [J]. Advanced Materials, 2025, 37 (34):2505132.
[12] Lei Tongda, Wang Yongheng, Zhang Qingsong, et al. Ultra-stretchable and anti-freezing ionic conductive hydrogels as high performance strain sensors and flexible triboelectric nanogenerator in extreme environments [J]. Nano Energy, 2024(126):109633.
[13] Min Weixing, Li Lengwan, Wang Mingli, et al. Mastering the Copolymerization Behavior of Ethyl Cyanoacrylate as Gel Polymer Electrolyte for Lithium-metal Battery Application [J]. Angewandte Chemie International Edition, 2025, 64 (13):e202422510.
[14] Zhuang Wubin, Wang Zihan, Li Chaowei, et al. Acidic Hydrogel Enables Full-Period Mn^{2+}/MnO_2 Conversion in High-Energy Quasi-Solid-State Zn-MnO_2 Batteries [J]. Advanced Materials, 2026, 38 (13), e22827.
[15] Liu Ruiqi, Wan Fu, Liu Bowen, et al. A robust TPU/PVA semi-interpenetrating polymer network gel electrolyte enabling high-performance zinc-ion batteries [J]. Applied Surface Science, 2026(731):16441.
[16] Yan Yichen Duan Sidi, Liu Bo, et al. Tough Hydrogel Electrolytes for Anti-Freezing Zinc-Ion Batteries [J]. Advanced Materials, 2023, 35 (18):2211673.
[17] Zhao Wei, Zhang Yan, Liu Qingsong, et al. Entropy-Modulated Short-Chain Cathode for Low-Temperature All-Solid-State Li–S Batteries [J]. Angewandte Chemie International Edition, 2025, 64 (1):e202413670.
[18] Li Xiangye, Wang Dahui, Ran Fen, et al. Key approaches and challenges in fabricating advanced flexible zinc-ion batteries with functional hydrogel electrolytes [J]. Energy Storage Materials, 2023(56):351–393.
[19] Wang Zhenwu, Heck Matthias, Yang Wenwu, et al. Tough PEG gels by In Situ Phase Separation for 4D Printing [J]. Advanced Functional Materials 2024, 34 (20):2300947.
[20] Zheng Kun, Zhang Yang, Wang Jialin, et al. Custom hydrogen-bond network grants hydrogel superior zinc-anode stability [J]. Chemical Engineering Journal, 2026(530):173219.
[21] Li Tao, Liu Jiating, Shu Hang.et al. High-Performance Deep Eutectic/Ionic Liquid Gels for Zinc-Ion Battery and Flexible Sensor Applications in Extreme Environments [J]. Advanced Functional Materials, 2026,36 (3):e14358.
[22] Zhuang Wubin, Wang Zihan, Li Chaowei, et al. Acidic Hydrogel Enables Full-Period Mn^{2+}/MnO_2 Conversion in High-Energy Quasi-Solid-State Zn-MnO_2 Batteries [J]. Advanced Materials, 2026, 38 (13): e22827.

Viser Technology Pte. Ltd.
Research and Application of Materials Science
DOI: 10.33142/rams.v7i2.19668

Research Article Open Access

β-Cyclodextrin is Used as a Solid-state Electrolyte Additive to Improve the Electrochemical Properties of Zinc-Ion Batteries

Bofan SU[†], Rong LI[†], Ying LIU, Haizhu SUN[*]

National & Local United Engineering Laboratory for Power Batteries, Faculty of Chemistry, Northeast Normal University, Changchun Jilin 130024, China

[*]***Corresponding Author:*** *Haizhu SUN, E-mail: sunhz335@nenu.edu.cn*
[†]**Co-first Authors**: *Bofan SU, Rong LI*

Abstract

Solid-state zinc-ion batteries (SSZIBs) have become a promising alternative energy storage system in the field of large-scale energy storage and flexible electronics due to their high safety, low cost, environmental friendliness and excellent theoretical specific capacity. However, there are still bottlenecks such as low ionic conductivity at room temperature, high solid-solid interface impedance, and poor zinc dendrite growth and interface stability. In order to solve these problems, polyethylene oxide (PEO) based solid-state electrolyte was used, and its polymer skeleton structure can inhibit the formation of zinc dendrites. However, PEO-based solid electrolytes still have defects such as insufficient ionic conductivity at room temperature and insufficient interface contact, which need to be further improved by functional additives. With its unique caged supramolecular structure, β-cyclodextrin can form host-guest complexes with zinc ions, significantly improving the ionic conductivity of PEO-based solid electrolytes. In this study, β-CD was introduced into the system as a modified additive, and the optimized β-CD solid-state electrolyte Zn||Zn was used Zn symmetric batteries exhibit an ultra-long cycle life of 675 h at a current density of 10 mA cm^{-2} and a capacity density of 1 mAh cm^{-2}, and an ultra-long cycle life of 813 h at a current density of 4 mA cm^{-2} and a capacity density of 1 mAh cm^{-2}. For Zn||I_2 cell, with an initial discharge specific capacity of about 144.51 mAh g^{-1} at a current density of 0.5 A g^{-1}, still maintains 91% capacity after 1800 cycles. This study not only provides a feasible scheme for zinc anode stabilization, but also confirms that β-CD provides a practical technical path for the practical application of PEO solid-state electrolyte batteries.

Keywords: *β-cyclodextrin; PEO solid electrolyte; zinc anode dendrite inhibition; interface control*

1 Introduction

In recent years, solid-state zinc-ion batteries (SSZIBs) have attracted widespread attention in the field of large-scale sustainable energy storage due to their high safety, low cost, environmental friendliness, and high theoretical capacity [1]. However, the practical application of SSZIBs is still plagued by many bottlenecks, such as zinc dendrite growth caused by uneven zinc ion deposition [2], as well as problems of high solid-solid interface impedance and interfacial side reactions (such as metal corrosion), which significantly reduce the coulombic efficiency (CE) and cycle life of the battery, severely restricting its commercialization process [3].

To overcome the key challenges of SSZIBs, researchers have developed a series of effective strategies, including zinc anode substrate modification, artificial interface protection layer construction, electrolyte system optimization, and research and development of new solid-state electrolytes [4]. Among the many technical routes, solid-state electrolyte modification and the introduction of functional additives have shown irreplaceable practical value in regulating interface behavior, optimizing ion transport, and improving battery performance due to their outstanding advantages such as no need for complex equipment, low modification cost, and good compatibility with existing industrial processes, and have become the most promising solutions for large-scale promotion [5]. Organic additives have attracted widespread attention due to their good dispersion in solid electrolytes and their unique regulatory mechanisms [6]. Most organic molecules have a strong affinity for zinc matrix and Zn^{2+}, which can preferentially adsorb on the surface of zinc anode, effectively hinder the disordered growth of zinc dendrites and alleviate interfacial side reactions, and improve the interfacial contact between solid electrolyte and electrode, thereby significantly improving the overall performance of SSZIBs [7]. For example, Wang et al. reported a strategy to regulate zinc ion deposition

Received: October 16, 2025; Accepted November 28, 2025

orientation while inhibiting side reactions by β-cyclodextrin (β-CD). The macrocyclic supramolecular cyclodextrin with hydrophobic cavity and hydrophilic surface can be horizontally adsorbed to the surface of the zinc anode, effectively shielding the charge on the electrode surface, standardizing the diffusion path of zinc ions, and allowing them to be horizontally epitaxial deposited at the lowest non-energy position.

Among various organic molecules, β-CD is a typical cyclic oligosaccharide, with a unique hydrophobic cavity structure and a large number of hydrophilic hydroxyl groups distributed on the outer surface, showing excellent dispersion and chemical stability [8]. Its rich hydroxyl group can be used as a zincophilic site, which strongly interacts with Zn^{2+} and electrolyte components, reconstructs the Zn^{2+} transport pathway, optimizes ion transport kinetics, and guides the uniform deposition of Zn^{2+} [9]. Its unique cavity structure can encapsulate active small molecules, further inhibit the electrode/electrolyte interface side reaction, improve interface stability, and provide a good material basis for the optimization of SSZIBs performance [10].

However, the systematic research on the application of β-CD as a multifunctional additive to SSZIBs solid electrolyte systems is still insufficient, and its regulatory mechanism on the stability of zinc anode, solid electrolyte ionic conductivity and overall electrochemical performance of batteries still needs to be further revealed. In this work, β-CD is introduced into polyethylene oxide (PEO) based solid-state electrolytes as green and efficient functional additives to solve the problems of instability, high interface impedance and insufficient ionic conductivity of SSZIBs zinc anode. The effects of β-CD on Zn^{2+} solvation structure, ion transport kinetics, zinc deposition behavior and interfacial stability were systematically studied. This study is expected to provide a simple and effective strategy for constructing highly stable and long-life SSZIBs, and broaden the application of cyclodextrin-based materials in the field of electrochemical energy storage. Zn||Zn assembled with PEO electrolyte with β-CD The Zn symmetric battery achieves an ultra-long cycle life of 675 h under the condition of 10 mA cm^{-2} current density and 1 mAh cm^{-2} capacity density, and a cycle life of 813 h under the condition of 4 mA cm^{-2} current density and 1 mAh cm^{-2}. For Zn||I_2, with an initial discharge specific capacity of about 144.51 mAh g^{-1} at a current density of 0.5 A g^{-1}, still maintains 91% capacity after 1800 cycles

2 Experimental Section

2.1 Materials

The experimental reagents selected in this experiment were polyethylene oxide (PEO), β-cyclodextrin (β-CD) (96%), zinc trifluoromethanesulfonate $Zn(CF_3SO_3)_2$, purity 98%, acetonitrile (CH_3CN, AR), all reagents were used directly without further purification. Ultrapure water is used in the experimental process.

2.2 Solid electrolyte preparation

Blank PEO solid electrolyte: weigh 1 g of PEO, 0.5 g of $Zn(CF_3SO_3)_2$, add to 30 mL of acetonitrile, and stir magnetically at room temperature for 6 h until completely dissolved, to obtain a homogeneous precursor; Pour into the Teflon mold and let it stand at room temperature for 48 h, and wait for the acetonitrile to fully volatilize and solidify to obtain a pure PEO solid electrolyte.

β-CD modified PEO solid electrolyte (PEO/β-CD): 1 g of PEO, 0.5 g of $Zn(CF_3SO_3)_2$, and 5 mg of β-CD were weighed, added to 30 mL of acetonitrile, and magnetically stirred at room temperature for 6 h until completely dissolved, and a homogeneous transparent precursor was obtained. The Teflon mold was poured into a PTFE mold and cured at room temperature for 48 hours to obtain a β-CD-modified PEO solid electrolyte.

2.3 Cell assembly

Solid-state electrolyte battery is assembled in an air environment, and is assembled in sequence according to the anode shell, zinc anode, solid electrolyte, cathode sheet, gasket, shrapnel, and cathode shell, and is pressed with a button battery sealer to ensure that the battery is well sealed. All batteries are coin cell type CR2032 cells.

2.4 Material characterization

Fourier transform infrared spectroscopy (FTIR) was used to characterize β-CD and solid-state electrolyte functional groups. Scanning electron microscopy (SEM) was used to observe the surface morphology of the zinc anode after cycling. Electrochemical tests are performed at CHI660E electrochemical workstations.

2.5 Electrochemical measurements

Electrochemical impedance spectroscopy (EIS): amplitude 5 mV, frequency 0.01 Hz-1.0 MHz. Linear scanning voltammetry (LSV): scanning rate 1 mV s^{-1}, hydrogen evolution 0-0.5 V, oxygen evolution 0-3 V. Tafel curve: Sweep rate 1 mV s^{-1}, voltage -0.3-0.3 V. The chronometric current method (CA) records the current-time curve. Ionic conductivity by stainless steel gasket-solid electrolyte-stainless steel gasket battery combined with EIS test, formula:

$$\sigma = \frac{L}{R\,S}$$

Ionic conductivity (S cm^{-1}), L is the electrolyte thickness (cm), R is the impedance (Ω), and S is the contact area (cm^2).

The number of Zn^{2+} migrations is via Zn||Zn symmetrical battery combined with i-t curve with EIS test, formula:

$$t_{Zn^{2+}} = \frac{I_S\,(\Delta V - I_0\,R_0)}{I_0\,(\Delta V - I_s\,R_s)}$$

where $t_{Zn^{2+}}$ is the Zn^{2+} migration number, ΔV is the polarization voltage, I_0 is the initial current, *Is* steady-state current, and R_0 and *Rs* are impedance before and after polarization.

Half-cell cyclic voltammetry (CV): Scan rate 2 mV s^{-1}, voltage range -0.2-0.4 V.

3. Results and Discussion

3.1 Characterization of solid-state electrolytes and analysis of the mechanism of action of β-CD

As shown in Figure 1a, the characteristic peak of stretching vibration appears at 3200-3500 cm^{-1}, 2850-2950 cm^{-1} is the carbon-hydrogen bond telescopic vibration absorption peak, and 1000-1200 cm^{-1} belongs to the molecular backbone C-O-C, indicating that the molecular structure of β-CD is intact. XRD was used to investigate the β-CD. As shown in Figure 1b, a distinct broad peak is observed in the range of 1-30 °. The PEO and PEO/β-CD composite electrolytes were characterized. As shown in Figure 1c, the incorporation of β-CD leads to a blue shift. This is because the introduction of β-CD provides more contact sites for Zn^{2+}. As shown in Figure 1d, after the addition of β-CD, the intensity of the two characteristic diffraction peaks of PEO was significantly weakened and the peak shape was widened, and there was no obvious crystal diffraction peak of β-CD. The results showed that β-CD could effectively disrupt the regular arrangement of PEO molecular chains, inhibit crystal growth, and reduce the crystallinity of the system. The increase of the amorphous zone ratio can improve the motion ability of polymer chain segments and construct a continuous ion transport channel, which is conducive to accelerating the migration rate of zinc ions.

Figure 2. shows a SEM comparison image of PEO/β-CD composite electrolyte and pure PEO electrolyte, which is used to visually reflect the microscopic morphological differences of the materials. PEO/β-CD composite electrolyte (Figures 2a-b): At 50 μm and 20 μm, the sample surface showed a uniform, dense, and continuous morphology, with no obvious holes, cracks, or phase separation. This indicates that β-CD has good dispersion in the PEO matrix, and the two form a homogeneous composite system through intermolecular interaction, constructing a continuous ion transport path. Pure PEO electrolyte (Figure 2c-d): The surface of pure PEO is rough, with obvious wrinkles, agglomeration and even microcracks, which is caused by its high crystallinity leading to regular stacking of chain segments and stress concentration. This inhomogeneous structure can easily cause ion transport path interruptions and affect electrolyte performance. In contrast, the introduction of β-CD significantly improved the microscopic morphology of PEO-based electrolytes, inhibited the crystal agglomeration of PEO, and formed a more uniform and dense film structure, which was mutually confirmed by the results of XRD and FTIR, and provided favorable conditions for improving the ionic conductivity and interface stability of the electrolyte.

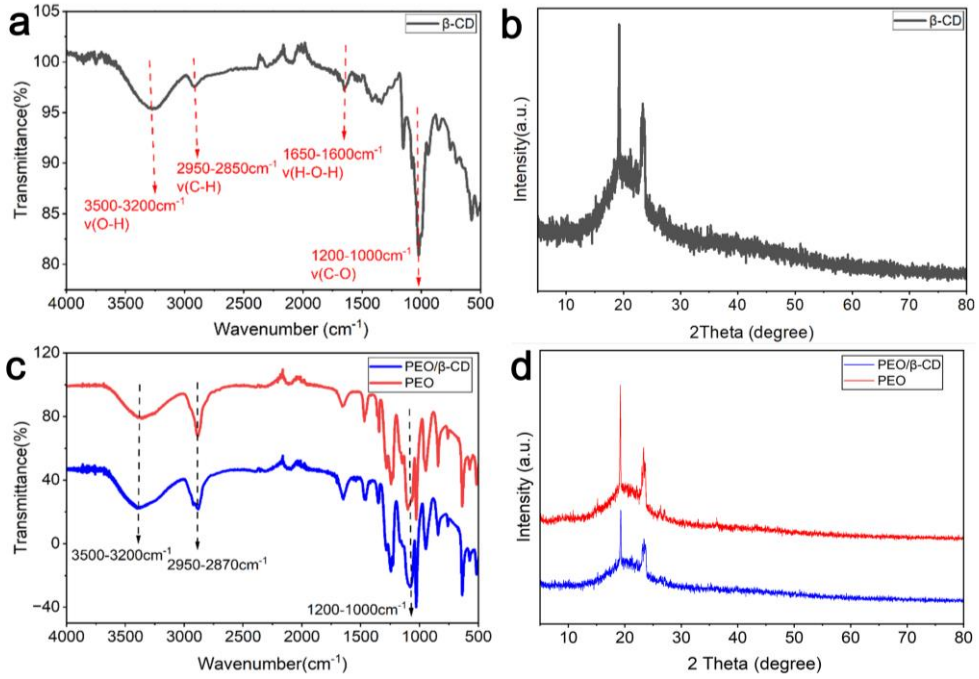

Figure 1 (a) FTIR spectra of pure β-CD. (b) XRD pattern of pure β-CD. (c) FTIR spectra of pure PEO and PEO/β-CD composite electrolyte. (d) XRD patterns of pure PEO and PEO/β-CD composite electrolyte

3.2 Effect of β-CD on the electrochemical properties of PEO solid electrolytes

Firstly, the electrochemical stability windows of PEO and PEO/β-CD composite electrolytes were evaluated via LSV. As shown in Figure 3a-3b, the introduction of β-CD greatly broadens the electrochemical stability window of the PEO/β-CD composite electrolyte. The negative voltage range shifts from -0.5 V to -1.0 V, while the positive voltage range expands from 1.80 V to 2.25 V, exhibiting a wider electrochemical stability window. This indicates that the incorporation of β-CD effectively improves the oxidation resistance of the PEO matrix, allowing the electrolyte to maintain chemical stability within a broader voltage range and thereby providing a safer and more stable operating environment for batteries. Figure 3c shows the AC impedance spectra of pure PEO and PEO/β-CD composite electrolytes for calculating ionic conductivity. The ionic conductivity of the pure PEO electrolyte was only 0.0198 mS cm^{-1}, while the PEO/β-CD composite electrolyte was significantly increased to 0.0482 mS cm^{-1}. It can be seen that the addition of β-CD reduces the impedance of the electrolyte body, destroys the highly crystalline structure of PEO, constructs a smoother zinc ion transport channel, and significantly improves the ion conduction ability.

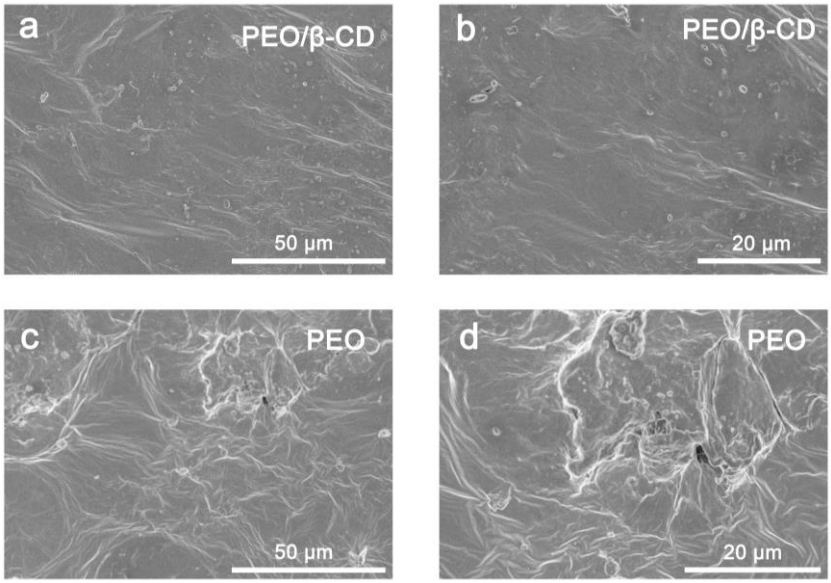

Figure 2 SEM image of PEO/β-CD electrolyte. (a) 50 μm. (b) 20 μm. SEM image of pure PEO electrolyte. (c) 50 μm. (d) 20 μm.

Interfacial kinetics was analyzed based on electrochemical impedance spectroscopy (EIS). Figure 3d shows the interface impedance comparison of the two electrolytes.The interface impedance of pure PEO electrolyte is 420000 Ω, and the load transfer resistance is high. The interfacial impedance of the modified PEO/β-CD composite electrolyte is 175000 Ω, which is small. The results show that β-CD optimizes the interface adhesion between the electrolyte and the electrode, reduces the charge transfer barrier, and facilitates the rapid migration of ions between interfaces. The zinc ion migration number (t_{Zn}^{2+}) determined by potentiostatic polarization combined with impedance method. Figure 3e shows the zinc ion migration number of pure PEO electrolyte is only 0.20, indicating that most of the current is contributed by anion migration, and the proportion of zinc ion directional transport is low, which can easily lead to serious concentration polarization and local current unevenness, and induce zinc dendrite growth. The t_{Zn}^{2+} of PEO/β-CD composite electrolyte increased to 0.55 (Figure 3f), which was significantly higher than that of the pure PEO system. This improvement is due to the complexation and binding effect of the cage structure of β-CD on anions, which effectively inhibits the migration of anions and promotes the directional transport of zinc ions, which is conducive to achieving uniform zinc deposition and inhibiting dendrite growth, thereby improving the cycle stability of the battery.

In conclusion, the electrochemical characterization results show that the β-CD modified PEO electrolyte shows significant advantages in electrochemical stability window, interface and body ion transport performance and zinc ion migration number, which corroborates the conclusions of the previous structural characterization, and fully proves the positive role of β-CD in optimizing the structure and performance of PEO-based solid electrolytes.

3.3 Effects of β-CD on zinc deposition behavior

Figure 4a shows the tafel polarization curves of pure PEO and PEO/β-CD composite electrolytes to characterize the corrosion current density of the zinc anode. The corrosion current density of the pure PEO

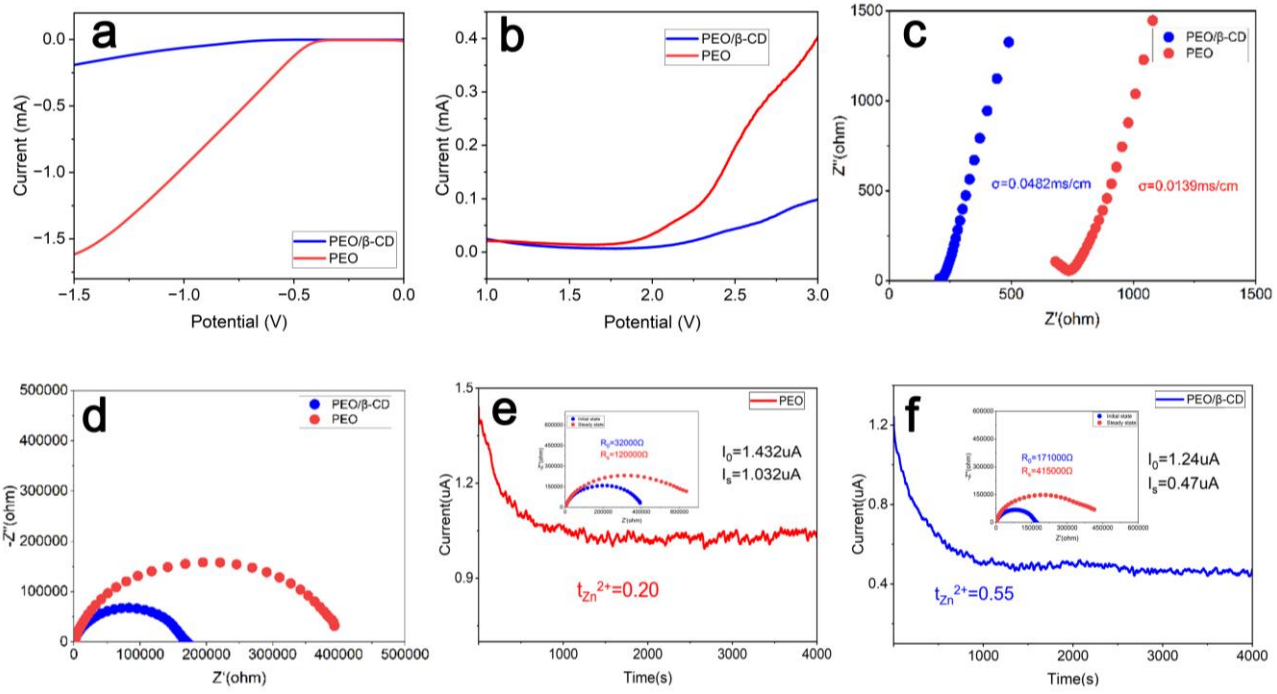

Figure 3 (a) LSV curves of PEO and PEO/β-CD electrolytes. (b) High-potential LSV curves of PEO and PEO/β-CD electrolytes. (c) EIS curves for ionic conductivity of PEO and PEO/β-CD electrolytes. (d) EIS of PEO and PEO/β-CD composite electrolyte. Fitting data of ion transference number. (e) PEO. (f) PEO/β-CD composite electrolyte.

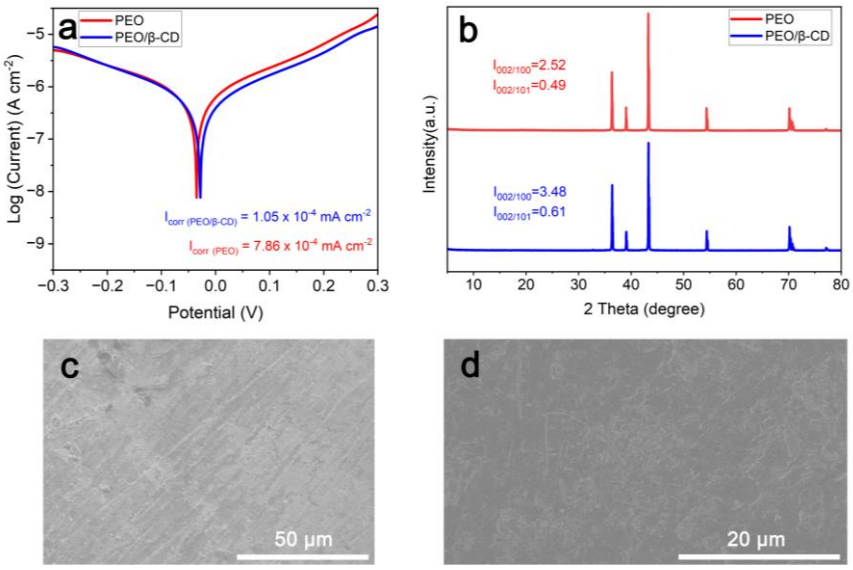

Figure 4 (a) Tafel polarization curves of Zn anodes in PEO and PEO/β-CD electrolytes. (b) XRD patterns of Zn anodes after cycling in PEO and PEO/β-CD electrolytes. (c) SEM image of Zn anode cycled in PEO electrolyte. (d) SEM image of Zn anode cycled in PEO/β-CD electrolyte.

system was 7.86×10^{-4} mA cm^{-2}, and after the introduction of β-CD, the corrosion current density of the PEO/β-CD system was reduced to 1.05×10^{-4} mA cm^{-2}, and the corrosion current was significantly reduced, indicating that β-CD effectively inhibited the side reaction and self-corrosion of the zinc anode, improved the interface stability of the zinc anode, and was conducive to the long-cycle cycle of the battery. Figure 4b shows the XRD patterns of the zinc anode after cycling in pure PEO and PEO/β-CD composite electrolytes, and the crystal plane orientation of zinc is analyzed by using the crystal surface strength ratio. In the pure PEO system, $I_{(002)}/I_{(100)}$ = 2.52 and $I_{(002)}/I_{(101)}$ = 0.49. After the introduction of β-CD, the intensity ratios of $I_{(002)}/I_{(100)}$ and $I_{(002)}/I_{(101)}$ are 3.48 and 0.61, respectively. The proportion of the (002) crystal plane increases significantly. The 002 crystal surface has a low zinc deposition energy barrier, which can induce uniform zinc

deposition along the horizontal direction parallel to the electrode surface, and effectively inhibit vertically growing zinc dendrites. β-CD regulates the crystal plane orientation of zinc, preferentially induces the optimal growth of 002 crystal plane, optimizes zinc deposition behavior, constructs a flat and stable zinc anode interface, and greatly improves the cycle stability of the battery.

The SEM diagram of PEO/β-CD composite electrolyte (Figure 4c), with a flat and dense surface, uniform structure, significantly reduced defects, and a continuous ion transport channel, reduced body impedance, and increased ion conductivity, while constructing a stable electrode-electrolyte interface, inhibiting zinc dendrites, and improving cycle stability. Figure 4d shows the SEM diagram of pure PEO electrolyte, with uneven surface and messy texture, a large number of defects and grooves, discontinuous ion transport pathways, high body impedance, and low ion conductivity, which is easy to cause local zinc dendrite growth.

3.4 Effect of β-Cyclodextrin on the stability of zinc anode

Figure 5a shows the long-cycle comparison curves of symmetrical batteries between pure PEO and PEO/β-CD composite electrolytes under the conditions of current density 10 mA cm^{-2} and capacity of 1 mAh cm^{-2}. Severe voltage fluctuations and polarization distortions occur in the pure PEO system at the beginning of the cycle, indicating that the interfacial side reactions and zinc dendrite growth have led to the rapid failure of the battery. The PEO/β-CD composite

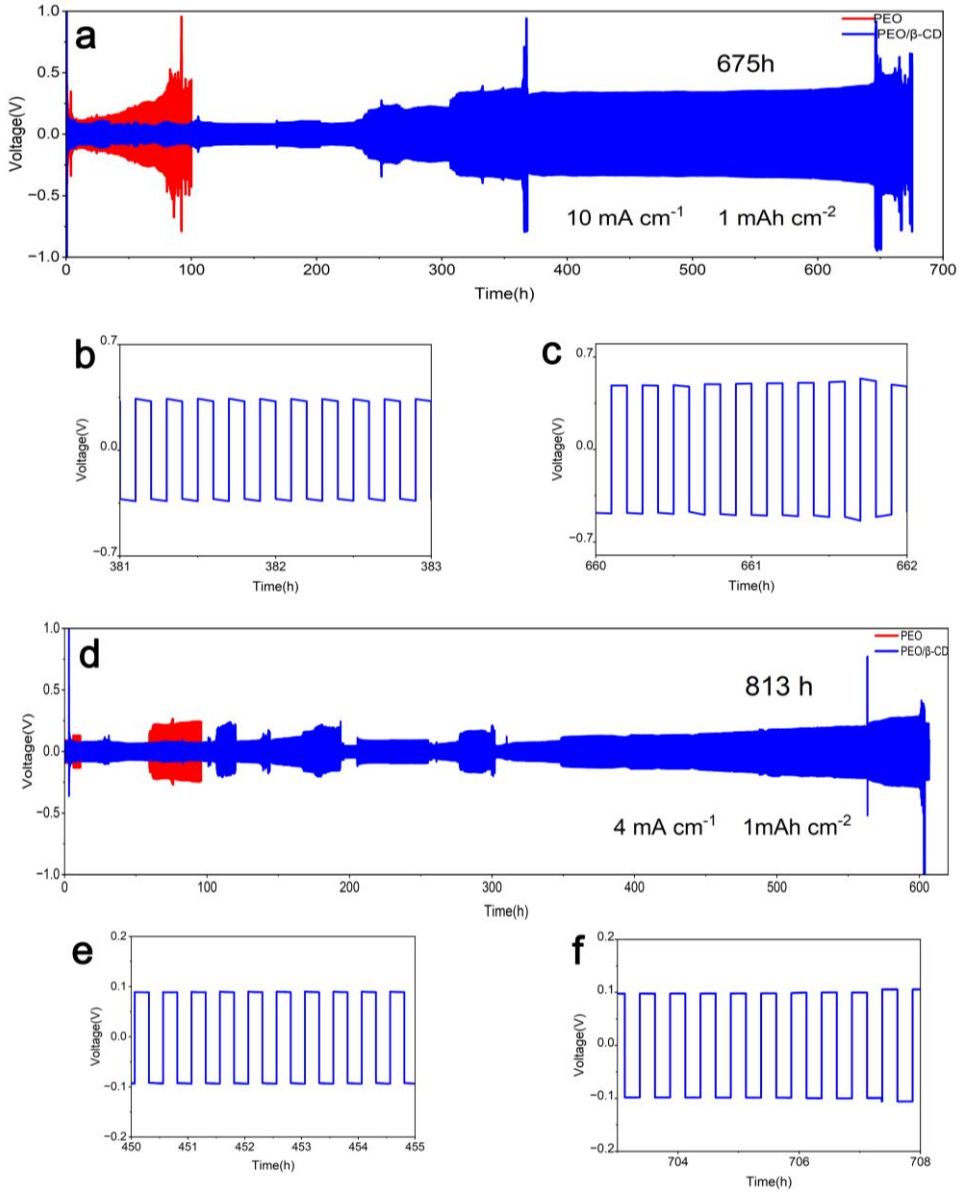

Figure 5 (a) Long-cycle performance of Zn||Zn cells at 10 mA cm^{-2}, 1 mAh cm^{-2}. Magnified voltage profiles at 10 mA cm^{-2}, 1 mAh cm^{-2}. (b) Middle cycle. (c) Late cycle. (d) Long-cycle performance of Zn||Zn cells at 4 mA cm^{-2}, 1 mAh cm^{-2}. Magnified voltage profiles at 4 mA cm^{-2}, 1 mAh cm^{-2}. (e) Middle cycle. (f) Late cycle.

electrolyte can be stably cycled for 675 h, the voltage curve is stable throughout the whole process, and the polarization voltage does not rise significantly, showing excellent interface stability and long cycle life. Figure 5b shows the voltage plateau amplification curve of the PEO/β-CD composite electrolyte at a current density of 10 mA cm^{-2} in the middle of the cycle. Figure 5c shows the amplification curve of the voltage platform at the end of the cycle under a current density of 10 mA cm^{-2} of the same system. The curve presents a clear, symmetrical rectangular platform, and the polarization voltage is stable at about ±0.5 V with no significant fluctuations or distortions. It shows that the zinc deposition/dissolution process is highly reversible, the interface polarization is stable, there is no voltage abnormality caused by dendrite growth or side reactions, and the interface state remains good. It was proved that after long-term cycling, the composite electrolyte could still maintain a stable interface environment, effectively inhibit dendrite puncture and interface deterioration, and showed excellent long-period interface stability. Figure 5d shows the long-cycle comparison curves of symmetrical PEO and PEO/β-CD composite electrolyte under the conditions of current density of 4 mA cm^{-2} and capacity of 1 mAh cm^{-2}. The pure PEO system has violent voltage fluctuations at the beginning of the cycle and fails quickly, indicating that the interfacial side reactions and dendrite growth lead to rapid deterioration of the battery. The PEO/β-CD composite electrolyte can be stably cycled for 813 h, and the voltage curve is stable throughout the process, and the polarization does not increase significantly, indicating that the composite electrolyte can also regulate zinc deposition behavior for a long time, inhibit dendrite and side reactions, and significantly extend the battery life under low and medium current density. Figure 5e shows the voltage plateau amplification curve of the PEO/β-CD composite electrolyte at a current density of 4 mA cm^{-2} in the middle of the cycle. Figure 5f shows the amplification curve of the voltage platform at the end of the cycle under the current density of 4 mA cm^{-2} of the same system. The voltage platform is symmetrical and regular, and the polarization voltage is stable at about ±0.1 V, which is much lower than the polarization value at high current density, indicating that the interfacial reaction is better at low and medium currents, and the zinc deposition/dissolution process is more uniform and stable.

3.5 Effect of β-CD on full cell performance

Figure 6a presents the cyclic voltammetry curves of Zn||I_2 full cell in PEO and PEO/β-CD composite electrolyte. Both sets of curves show a clear pair of oxidation/reduction peaks, corresponding to the embedding/de-intercalation of zinc ions. The peak current of the PEO/β-CD system is higher, the peak shape is sharper, and the potential difference of the redox

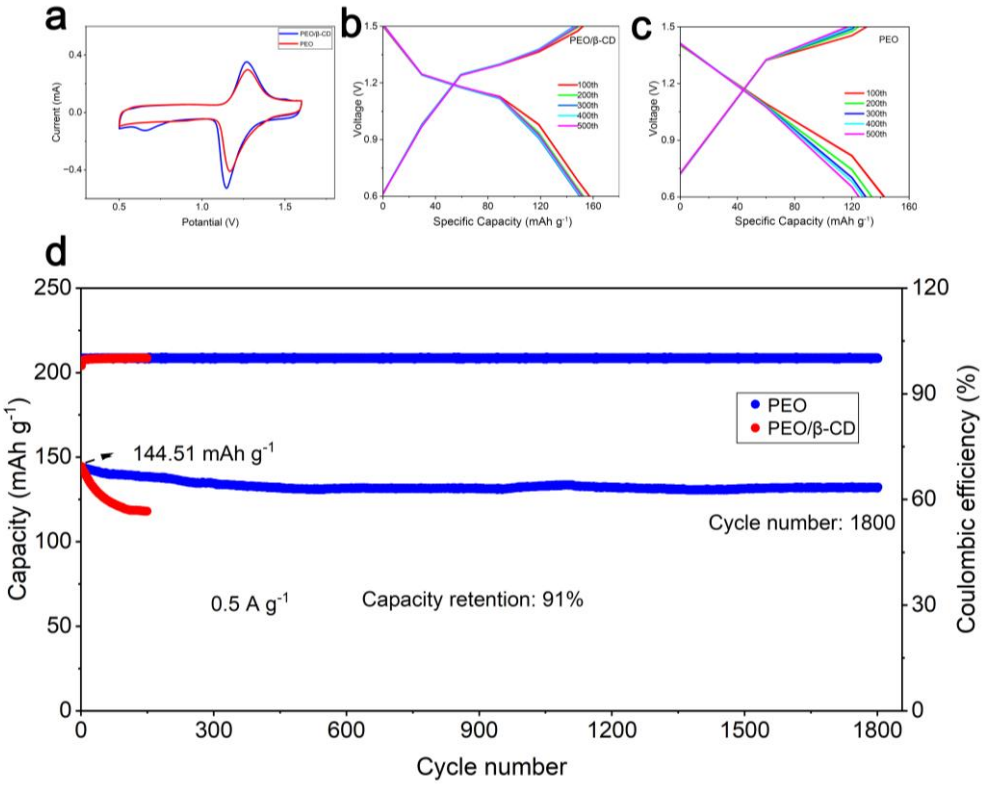

Figure 6 (a) CV curves of Zn||I_2 full cells with PEO and PEO/β-CD electrolytes. (b) GCD curves of PEO-based full cell at different cycles. (c) GCD curves of PEO/β-CD-based full cell at different cycles. (d) Long-cycle performance of full cells with PEO and PEO/β-CD electrolytes at 0.5 A g^{-1}

peak is smaller, indicating that the reversibility of the system is better, the polarization is lower, and the zinc ion transport kinetics are better.

The current constant charge-discharge (GCD) curve exhibits excellent stability. The current constant charge-discharge curve of PEO/β-CD battery showed excellent stability (Figure 6b): the charging and discharging platform was still clear after multiple cycles, the capacity decay was slow, and the voltage polarization did not increase significantly, indicating that the β-CD modification effectively stabilized the electrode-electrolyte interface, inhibited the zinc dendrite and side reaction, and improved the reversibility and structural stability. In contrast, pure PEO Zn||I_2 cells (Figure 6c) have rapid deterioration of battery performance due to rapid capacity decay, continuous intensification of polarization, gradual deformation of the platform, and serious interfacial side reactions and dendrite growth with the increase of cycle times. Figure 6d shows the long-cycle performance comparison curve of Zn||I_2 cell at 0.5 A g^{-1} current density. The specific capacity of the pure PEO system decays rapidly at the beginning of the cycle, and the battery fails quickly after 170 cycles. The initial specific capacity of the β-CD composite electrolyte system is 144.51 mAh g^{-1}, and after 1800 long cycles, the capacity retention rate is still as high as 91%, and the coulomb efficiency is always close to 100%, showing excellent long-cycle stability and reversibility.

It was shown that the β-CD composite electrolyte significantly improved the reaction kinetics and interface stability of Zn||I_2 cell, effectively inhibited the growth and side reactions of zinc dendrites, greatly improved the reversible charge-discharge performance and long cycle life of the battery, and provided a feasible solution for the construction of high-stability zinc-based whole batteries.

4 Conclusion

In this work, PEO-based solid electrolytes were taken as the research object, and the regulatory mechanism of β-cyclodextrin modification on the interface stability and electrochemical properties of zinc-ion batteries was systematically explored. Through structural characterization and electrochemical testing, it was confirmed that the introduction of β-CD effectively destroyed the high crystallinity of PEO, increased the amorphous region, and constructed a continuous and smooth transport channel for zinc ions, which significantly improved the conductivity of electrolyte ions. Tafel plot and XRD analysis showed that β-CD could reduce the corrosion current of the zinc anode, induce the optimal deposition of zinc along the (002) crystal plane, inhibit the growth of vertical dendrites, and construct a flat and stable electrode interface. The test results of zinc symmetric batteries show that the PEO/β-CD composite electrolyte can achieve ultra-long stable cycles of 813 h and 675 h at the current density of 4 mA cm^{-2} and 10 mA cm^{-2}, respectively, with an areal capacity of 1 mAh cm^{-2}. And the voltage polarization is always maintained at a low level, showing excellent interface stability and cycle reversibility. On this basis, the Zn||I_2 cell test further verifies the effectiveness of the modification strategy. After 1800 cycles at a current density of 0.5 A g^{-1}, the PEO/β-CD-based Zn||I_2 cell retains a high capacity retention of 91% with an initial capacity of 144.51 mAh g^{-1}. This performance is significantly superior to that of the pure PEO system, fully demonstrating the critical role of β-CD modification in enhancing the long-cycle stability of the battery. In this study, the synergistic improvement of the ionic conductivity of PEO solid-state electrolyte and the interface stability of zinc anode was realized by β-CD modification, which provided an effective interface regulation strategy for the development of high-performance and long-life zinc-based solid-state batteries.

Acknowledgements: This work was supported by Jilin Province Science and Technology Development Plan Project (International cooperation 20240402073GH), the National Natural Science Foundation of China (22275030).

References

[1] ZHU Y, HAN T, LIN X, ZHANG H, HU C, LIU J. [J]. Chem Commun, 2023(59):2640–2643.

[2] MA L, CHEN S, LI N, et al. Hydrogen-Free and Dendrite-Free All-Solid-State Zn-Ion Batteries [J]. Advanced Materials, 2020(32): 1908121.

[3] ZHANG Y, ZHANG T, GAO S, et al. 3D porous polymer framework induced by molecular bridging reaction enables quasi-solid zinc-ion batteries [J]. Science China Chemistry, 2026(25): 11426.

[4] ZHANG H, WU H, WANG L, et al. Benzophenone as indicator detecting lithium metal inside solid state electrolyte [J]. Journal of Power Sources, 2021(492): 229661.

[5] SU J, PASTA M, NING Z, et al. Correction: Interfacial modification between argyrodite-type solid-state electrolytes and Li metal anodes using LiPON interlayers [J]. Energy & Environmental Science, 2023(16): 698.

[6] YANG S, MENG T, WANG Z, et al. Polymeric ionic conductor networks enable stable cycling of high-voltage lithium metal batteries using solid-state poly-ether electrolytes [J]. Journal of Materials Chemistry A, 2024(12): 29630.

[7] ZHOU T, LEI Y, XUE Y, et al. Application, improvement and prospective advancements of solid electrolytes in zinc-ion batteries [J]. Journal of Energy Storage, 2025(139): 118765.

[8] CHEN S, FENG F, YIN Y, et al. A solid polymer electrolyte based on star-like hyperbranched β-cyclodextrin for all-solid-state sodium batteries [J]. Journal of Power Sources, 2018(399): 363-371.

[9] ABDELHAY A H, BANI-YASEEN A D. Exploring cyclodextrin-driven advancements in aqueous Zn-ion battery: A review [J]. Carbohydrate Polymers, 2025(349): 123041.

[10] GUO H, SU Y, ZHAO J, et al. Ultra-stable and long-life zinc anodes enabled by porous cyclodextrin-based polymer coatings [J]. Journal of Energy Storage, 2025(123): 116856.

Publisher: Viser Technology Pte. Ltd.

URL: www.viserdata.com

Add.:195 Pearl's Hill Terrace, #02-41,

Singapore 168976

ISSN 2661-4456

02